STABILITY BOUNDARY ANALYSIS OF GRID-FORMING AND GRID-FOLLOWING INVERTERS

Xi Luo[1], Efstratios Batzelis[1], Abhinav Singh[1], Georgia Saridaki[2], Panos Kotsampopoulos[2]*

[1]*School of Electronics and Computer Science, University of Southampton, Southampton, UK*
[2]*School of Electrical and Computer Engineering, National Technical University of Athens, Greece*
**xi.luo@soton.ac.uk*

Keywords: GRID STRENGTH, STABILITY CRITERIA, GRID-FOLLOWING (GFL) INVERTER, GRID-FORMING (GFM) INVERTER, SMALL-SIGNAL ANALYSIS.

Abstract

Stability issues and oscillations associated with inverter-based resources (IBRs) are of increasing concern in inverter-dominated power systems. This study explores the stability boundary of grid-following (GFL) and grid-forming (GFM) inverters and performs a sensitivity analysis for the most relevant control and grid parameters. A stability boundary tracking (SBT) algorithm is proposed, which can identify the stability boundary relating up to three parameters of interest for both GFL and GFM inverters. This boundary is then illustrated as two-dimensional stability curve or three-dimensional stability surface to facilitate understanding the impact of certain parameters on the stability margin. A comprehensive sensitivity analysis of different controller parameters as well as power factor and line R/X ratio draws parallels on their impact to GFL and GFM stability.

1. Introduction

With the increasing penetration of renewable energy resources, power grids with long-distance transmission lines suffer from weak grid issues, such as voltage fluctuations and instability. Grid impedance typically indicates the strength of the grid and is conventionally categorized by the short-circuit ratio (SCR) [1]. IEEE Standard 1204-1997 defines the grid strength as: very weak (SCR≤2), weak (2<SCR<3), and strong (SCR>3) [2]. The issue of grid-connected inverters operating in grid-following (GFL) or grid-forming (GFM) mode exhibiting different stability behaviour under different grid strengths has been raised. It is emphasized that GFL tends to be unstable in weak grids, while GFM may lose synchronization in very stiff grids [3]. Relevant oscillatory phenomena reported in both low and high frequencies [4] usually result from the multi-layer inverter control and its interaction with the grid and other components. A comprehensive comparative study of the stability attributes of GFL and GFM is therefore essential.

Current research has explored the stability of GFL and GFM inverters connected to the grid with different SCRs and validated by time domain simulations or experiments. For example, it is suggested in [3] that GFL fails to maintain stability when SCR is less than 1.58, and GFM struggles for SCR higher than 11.67. Also, the cases in [1] illustrate that the stability margins for GFL and GFM are less than 2 and greater than 8, respectively. Such empirical observations, however, are case-specific and cannot be generalized easily.

A sounder alternative is to formally identify the *stability boundary* relating to certain parameters of interest, i.e., the values of these parameters that set the system marginally stable. The stability boundary demarcates the stable from the unstable region in the N-dimensional space, where N is the number of parameters of interest. Some studies in the literature study such boundaries, such as the relationship between droop coefficient and line impedance in [5]; this relation shows that the larger the droop coefficient in GFM, the worse the stability and therefore higher impedance values are required to ensure stability. In [6], the study investigates the effects of phase-locked loop (PLL) in GFL systems and suggests that at lower SCRs, boosting PLL gains can enhance system stability. The study in [7] further derives a symbolic stability boundary equation for GFL, which reveals that control loop bandwidth interactions lead to instability in weak grids. However, such specific observations cannot lead to universal conclusions; what is missing is a structured way to identify the stability boundary, and a comprehensive sensitivity analysis for all parameters for both GFL and GFM inverters.

In addition, most studies assume that transmission lines are purely inductive. However, authors in [8] use a reduced-order state-space model to derive stability boundaries for different R/X values and demonstrate that there is some stability impact from the resistive part of transmission lines. Different power factors are also employed in the stability analysis in [1]. Therefore, it is also of significance to study the stability impact of the aforementioned grid settings and power factor.

To address this research gap, a methodical exploration of the stability boundary in GFL and GFM inverters is proposed in this paper. The main contributions of this study are:

- A new generic method to identify the stability boundary of up to three parameters;
- A comprehensive sensitivity analysis for all critical control parameters (droop coefficient, voltage controller gains, etc.) and relevant grid parameters (R/X ratio, leading/lagging power factor) on their stability effect;
- Drawing parallels on the stability impact of various parameters between GFL and GFM inverters.

Simulations on the 3-bus testbench are used to validate the findings of this study.

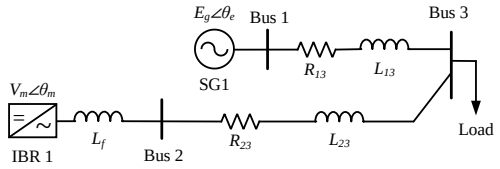

Fig. 1. The modified 3-bus testbench power system.

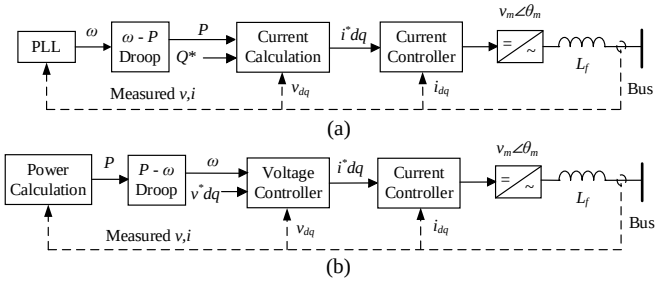

Fig. 2. System diagrams for (a) GFL and (b) GFM inverters.

2. Methodology

2.1 System configuration and inverter controls

The modified 3-bus power system [9,10] used in this study to investigate the dynamic behaviour of the inverter is shown in Fig. 1; the generator of bus 2 has been replaced by an inverter-based resource (IBR) for the purpose of this experiment. The inverter is connected to the grid via an L filter (L_f) and operates in either GFL or GFM control mode.

Fig. 2(a) depicts a typical GFL controller with droop-based frequency response [11]. The outer loop involves a phase-locked loop (PLL) for grid synchronization and frequency-droop control *P(f)* module for primary frequency response, while the inner loops translate the power setpoints to current commands that eventually drive the inverter output. The standard droop-based GFM controller is shown in Fig. 2(b) [12]. Here, the GFM scheme employs the droop function *f(P)* for both synchronization and frequency response, which forms its reference frequency and voltage actively, implemented at the connection point via a voltage and current controller.

The aforementioned droop control modules contain a low-pass filter (LPF) with a cut-off frequency f_c and a droop gain m_P (in per unit) defined as:

$$\omega - \omega_0 = -m_P(P - P_0), \qquad (1)$$

where ω_0 and P_0 denote the system nominal frequency and inverter power rating, and the LPF is used for power/frequency measurement [11]. Please note that for GFM the generated angular frequency will be $\omega = \omega_0 + m_P(P_0 - P)$, whereas the reference power in GFL will be $P = P_0 + (\omega_0 - \omega)/m_P$.

2.2 Stability boundary mapping

To investigate the system dynamic behaviour, the full-order state-space model of the entire 3-bus system is built and assessed stability-wise via small-signal analysis. The differential and algebraic equations (DAEs) of the inverter and synchronous generator can be found in [3] and [13]. The linearization is performed in MATLAB script with the linearize function. The eigenvalues of this system can

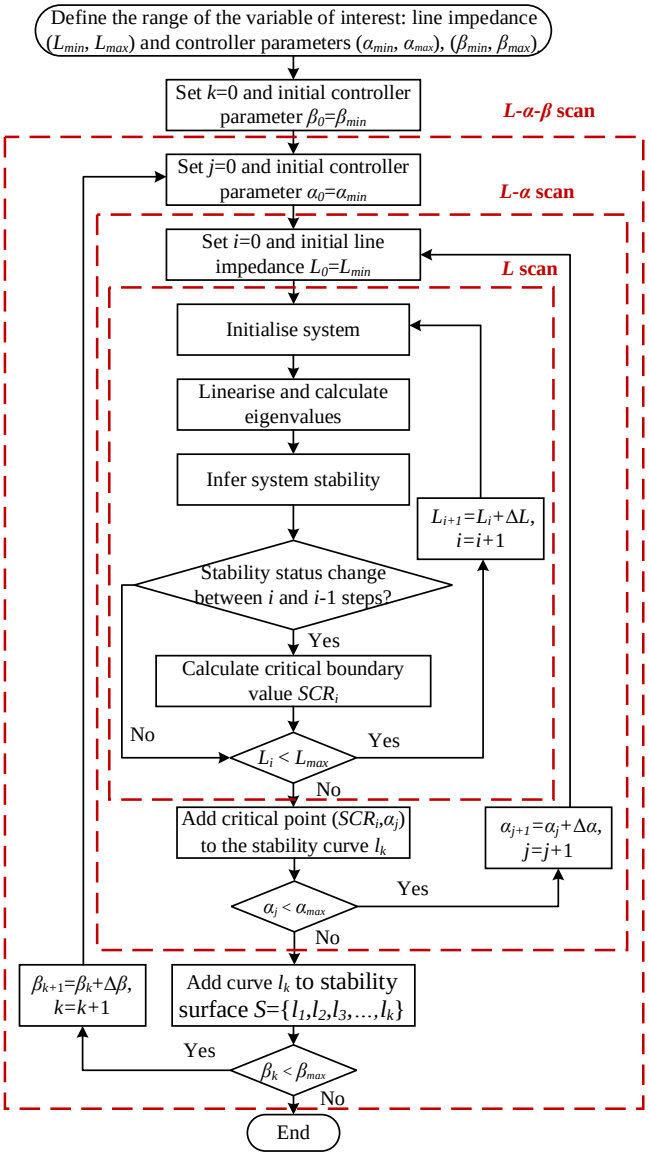

Fig. 3. Flowchart of the proposed SBT algorithm.

therefore be calculated, and if all the eigenvalues are situated in the left half-plane of the complex plane, the system is inferred to be stable at this equilibrium point. However, to identify the stability boundary, this process needs to be repeated several times for various parameters and operating points in a structured manner. Such a methodical approach is currently missing from the literature.

This paper introduces such a method, denoted as *Stability Boundary Tracking* (SBT) algorithm and shown in the flowchart of Fig. 3, which is able to calculate the multi-dimensional stability boundary of the system. The SBT algorithm is essentially a "grid search" of all parameters of interest, i.e. sampling the stability status for all possible combinations to form the stability boundary.

The flowchart starts by defining the range of variables of interest, i.e. the line impedance L and up to two controller parameters α and β, while the minimum value of each variable is set as the initial point L_0 and α_0, β_0. At this initial point, the

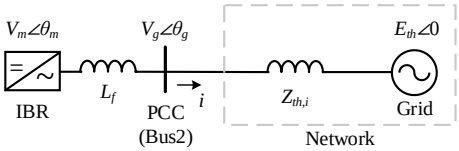

Fig. 4. Thévenin equivalent network.

Table I. Parameters of the system.

Parameters	Symbol	Values
System frequency	f_0	60 Hz
Base power	S_B	100 MVA
Transmission line 13 impedance	Z_{13}	$0.001 + j0.01$
Transmission line 13 impedance	Z_{23}	$0.001 + j0.01$
Reference inverter active power	P_0	1 pu
Reference inverter reactive power	Q_0	0 pu
Reference inverter voltage	v_0	1.01 pu
Droop coefficient	m_p	1% in GFL 5% in GFM
Low-pass filter cut-off frequency	f_c	20 Hz
PLL proportional gain	k_p	1
PLL integral gain	k_i	3800
Voltage control proportional gain	k_{pv}	5
Voltage control integral gain	k_{iv}	250
Current control proportional gain	k_{pi}	1.25
Current control integral gain	k_{ii}	10

system is initialised, linearized and the stability is inferred from its eigenvalues; then, this process is repeated for different line impedance values within the range (L_{min}, L_{max}) to observe when stability changes from stable to unstable or vice versa; when this happens, the relevant SCR is calculated and is treated as the *critical boundary value* SCR_i. This loop is referred to as "L scan" in the flowchart. The SCR is calculated via the Thévenin equivalent model (Fig. 4) [14]:

$$SCR_i = \frac{P_{SC}}{P_N} = \frac{|E_{th}|^2}{|Z_{th,i}|P_N} \quad (2)$$

where E_{th} and $Z_{th,i}$ are the equivalent Thevenin voltage source and series impedance. P_{SC} is the short-circuit power at the point of common coupling (PCC) and P_N is the nominal power of inverter. If the objective is to find this critical value (e.g. minimum SCR for a GFL connection), then the 1-D stability boundary has been identified and the process is complete.

In case a 2-D stability boundary is required to identify the relation between a control parameter α and SCR, then "L scan" needs to be repeated for different α_j values from α_{min} to α_{max}. The pairs (SCR_i, α_j) are then collated together to form the *stability curve* l_k, a process shown as "L-a scan" in the flowchart. If a 3-D stability boundary is required instead, then many such stability curves are produced for different β values within (β_{min}, β_{max}) to form the *stability surface* S (L-a-β scan). It is worth noting that the same flowchart can be used for 1-D, 2-D and 3-D stability boundaries by setting $\alpha_{min} = \alpha_{max}$ and/or $\beta_{min} = \beta_{max}$ accordingly to bypass the respective parameter scans.

3. Results

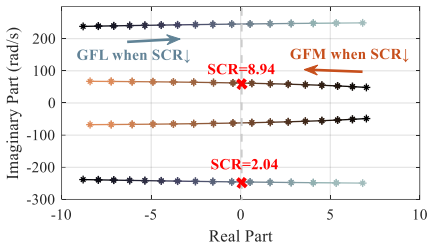

Fig. 5. Traces of critical eigenvalues for varying SCR.

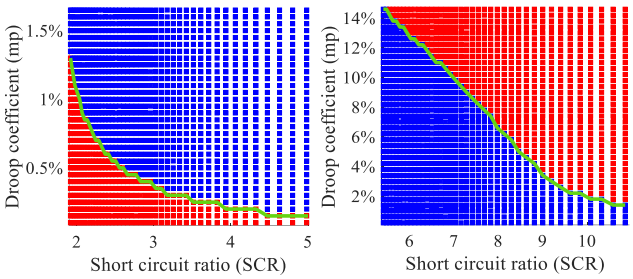

(a) (b)

Fig. 6. m_P vs. SCR stability boundary curves for (a) GFL and (b) GFM inverters. Blue and red dots indicate stable and unstable points respectively.

Table II. Critical eigenvalues and participation factors.

	GFL	GFM
SCR boundary point	2.04	8.94
Frequency (Hz)	39.10	9.87
Major part. factors	$\omega^{GFL}, \Delta\omega_{filt}^{GFL}, i_{dq}^{GFL}$	$\theta^{GFM}, v_{dq}^{GFM}, \Delta P_{filt}^{GFM}$

This section applies the SBT algorithm on the modified 3-bus system to visualize the various parameters impact on the stability of GFL and GFM inverters. First, the 1-D critical SCR is examined for one indicative case, followed by 2-D stability curves and 3-D stability surfaces relating different control parameters to SCR. The grid strength is modified by varying the impedance of line 23 and the control parameters considered are: the droop setting, the LPF cut-off frequency, the PLL gains (for GFL) and the voltage controller gains (for GFM). Finally, a sensitivity analysis is performed for different line R/X ratios and different power factors. The parameters of system components are given in Table I.

3.1 Critical SCR

The first case explores the stability of the system with varying line impedance L_{23} from 0.43 pu to 0.49 pu for GFL (from 0.01 pu to 0.13 pu for GFM), which corresponds to SCR decreasing. Fig. 5 illustrates the trajectories of dominant eigenvalues as SCR is reduced (the remaining eigenvalues are not affecting the stability and are omitted for simplicity). As expected, the eigenvalue pair of GFL moves towards the right half-plane, i.e. stability worsens as SCR decreases, whereas GFM stability improves. It is worth noting that the SCR value where the eigenvalues intersect the imaginary axis is identified as the critical stability boundary point. Table II lists these boundary points along with the main participating factors. The critical eigenvalues lie in the sub-synchronous range and depend mainly on the synchronization loops.

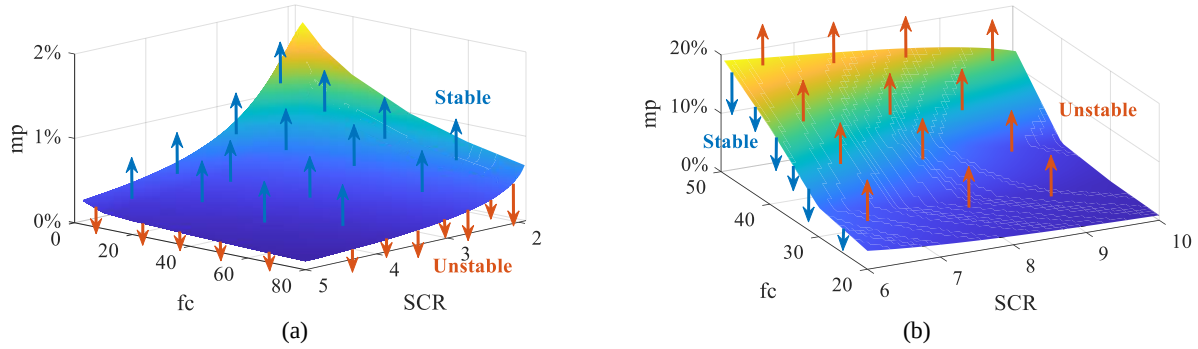

Fig. 7. m_P vs. SCR vs. f_c stability boundary surfaces for (a) GFL and (b) GFM. Blue and red arrows indicate stable and unstable spaces respectively.

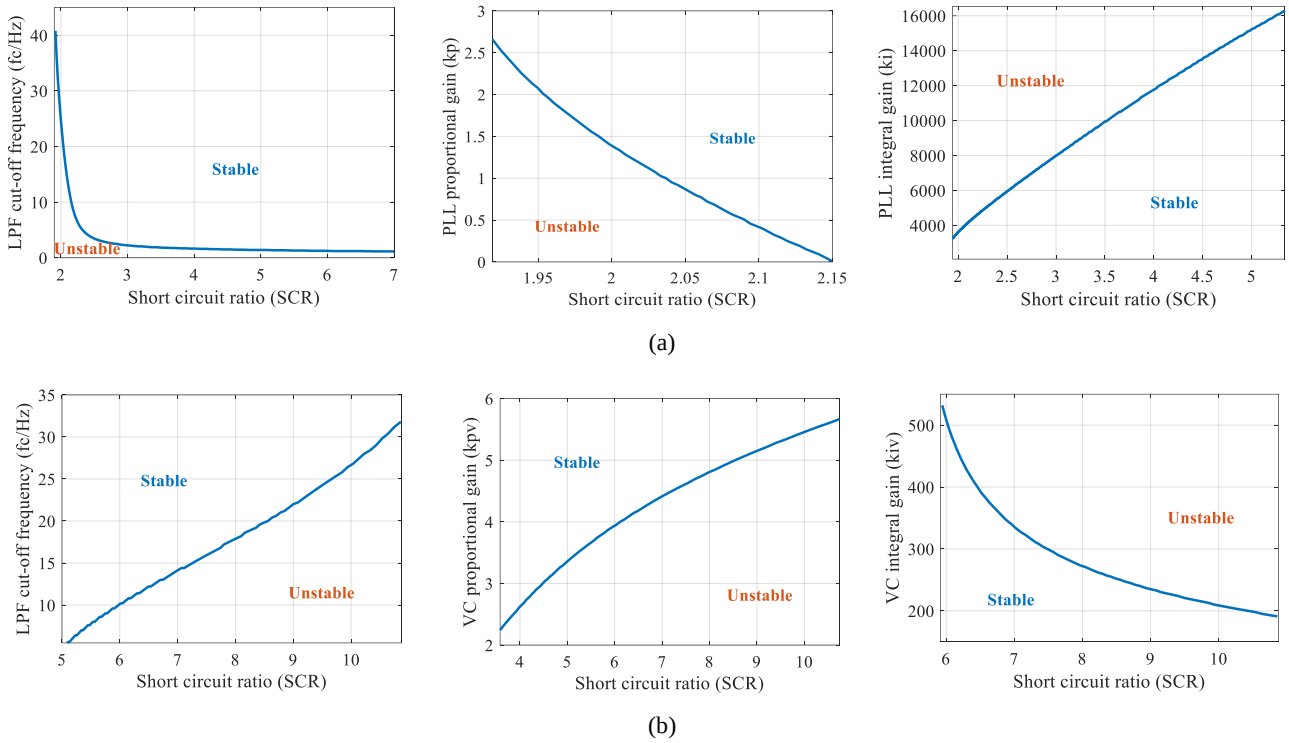

Fig. 8. Stability boundary curves of LPF cut-off frequency (f_c) and PLL controller parameters (k_{pv}, k_{iv}) for (a) GFL and (b) GFM.

3.2 Stability Boundary curve and surface

Fig. 6 shows the results of the SBT algorithm for the m_p-SCR stability curve, i.e. a 2-D stability boundary, for GFL and GFM systems. Every square marker in the plots corresponds to a certain combination of m_p and SCR, which makes the system either stable (blue colour) or unstable (red colour). The stability boundary can therefore be defined as the borderline between the stable and unstable regions, highlighted with the green curve in Fig. 6, and is the direct output of the SBT algorithm. In subsequent plots of 2-D stability boundary plots, only the stability curve itself is shown (i.e. the green curve) without the square markers for clarity.

Fig. 6(a) reaffirms literature observations that GFL performs better in stronger grids with smaller line impedance values, while GFM in Fig. 6(b) features a reversed trend. In addition, the shape of boundary lines implies that increasing m_P improves GFL stability, whereas it worsens GFM stability (stable and unstable regions reverse in the two plots – please see the definition of droop coefficient in Section 2.1). These findings are in line with literature observations [15].

The analysis was then extended to three dimensions, in which a third parameter was added to produce the m_P -SCR- f_c boundary. As an example, in Fig. 7, the blue and red arrows represent the stable and the unstable systems, respectively, forming a surface between them. The colour shading of the surface in Fig. 7(a) demonstrates that increasing m_P is not the sole method for improving GFL stability; it is also necessary to adjust f_c to an adequate level. Fig. 7(b) indicates that decreasing m_P and increasing f_c both lead to a larger stable region, i.e., the GFM stability margin increases.

3.3 Case studies: Sensitivity analysis of controller parameters

To explore the effect of the droop function, Section 3.2 first examines the relationship between the droop coefficient (m_P)

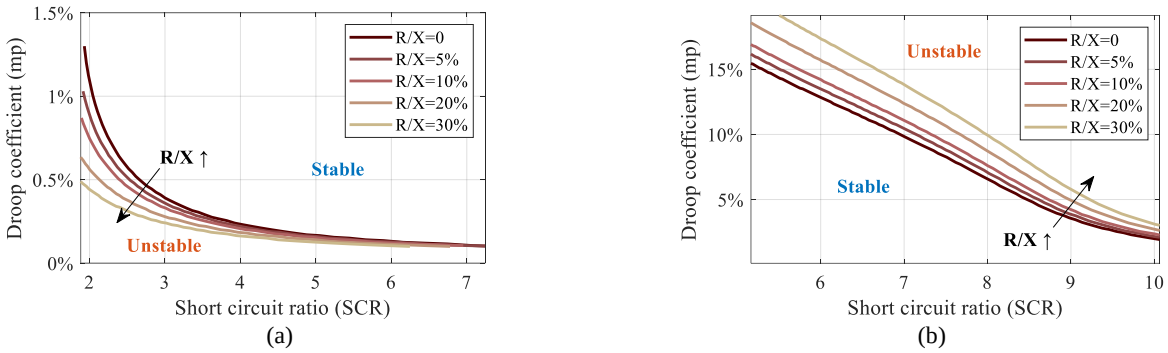

Fig. 9. Stability boundary results of m_P vs. SCR in (a) GFL and (b) GFM for different R/X ratios.

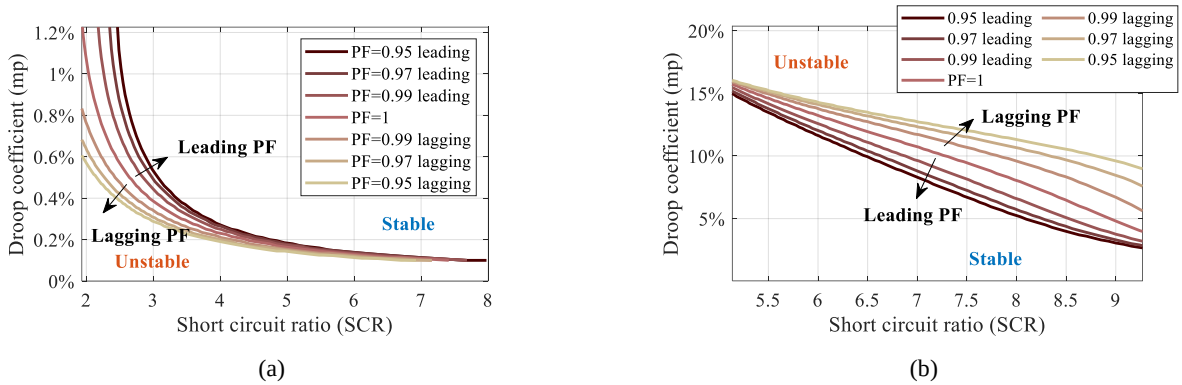

Fig. 10. Stability boundary results of m_P vs. SCR in (a) GFL and (b) GFM for different power factors set points.

and the grid strength which shows opposite trend on GFL and GFM stability. The stability characteristics of other controller parameters, including LPF cut-off frequency in droop control and the controller gains in both PLL and voltage control, are presented in Fig. 8. A first observation on grid strength impact reveals that GFL performs well with larger SCRs as it can easily track the grid voltage for power synchronisation, whereas GFM performs better at smaller SCRs when it can actively adjust the inverter frequency.

Further examination of Fig. 8 shows that the variation of the controller parameters greatly affects the stability region. In the GFL example, reducing f_c of LPF from 40 Hz to 1 Hz requires a stronger grid strength (above SCR=7) to maintain stability. When the cut-off frequency is decreased further, the system becomes unstable across all grid conditions. Similarly, reducing f_c in GFM expands the unstable region. This comparison reveals that increasing the f_c within a reasonable range enhances stability for both GFL and GFM. This is expected, as lower f_c entails longer time lag between measurement and actuation that is often detrimental in closed-loop control systems [16].

As seen in Fig. 8(a), when PLL parameters are taken into account, the GFL system stability worsens as k_p decreases below 2.6; also, a higher value of k_i is required as the grid becomes weaker. Fig. 8(b) shows that increasing k_{pv} from 3 to 5 can expand the feasible SCR stable range of GFM from 4.5 to 8.6, whereas an increase in k_{iv} reduces the stability region and even result in GFM getting unstable below SCR=3.6. These points suggest that both GFL and GFM systems require a critical balance between proportional and integral gains (increasing k_p or decreasing k_i) of the PLL/voltage controller. Again, these findings are in line with literature observations, but this is the first study to put these into a comparative framework for GFL and GFM.

3.4 Case studies: Sensitivity analysis of grid conditions

To explore the importance of other grid conditions, sensitivity analyses of the line R/X ratio and power factor were performed. The system was first tested at various line R/X ratios ranging from 0% to 30%, which represent the proportion of the resistive to inductive components of the transmission line. Next, the system's performance was assessed under different leading and lagging power factors (PF) for both GFL and GFM. These two cases aim at observing how the boundary curve varies with changes and evaluate their importance.

3.4.1 R/X ratio: The m_P vs. SCR stability curve is reproduced for different R/X ratios, as shown in Fig. 9. When the R/X ratio increases, the stable region expands in both cases. This implies that the presence of resistive part in transmission lines has a positive impact on system stability. Notably, there is insignificant impact for R/X up to 10%, which indicates that a purely inductive grid impedance is a valid assumption at low R/X grids such typical high voltage transmission systems.

3.4.2 Power factor: Fig. 10 shows the variation of the m_P vs. SCR stability boundary for different PF setpoints, assuming 100% apparent power injection in every case. From light to dark colours, the PF setting changes from lagging to leading. In both cases, the leading PF indicates a larger unstable region and tends to worsen the system stability. Furthermore, result in GFL indicates that PF has a greater impact under weaker

Table III. Summary of sensitivity analysis results. (Note that (+) indicates that SCR stability region improves as it increases; (−) is reversed meaning it decreases.).

Parameter increase	Stability impact	
	GFL	GFM
Droop coefficient m_P	(+)	(−)
LPF cut-off frequency f_c	(+)	(+)
PLL k_p/Voltage controller k_{pv}	(+)	(+)
PLL k_i/Voltage controller k_{iv}	(−)	(−)
R/X ratios	(+)	(+)
PF lagging → leading	(−)	(−)

grid conditions, whereas GFM presents a different story, i.e. the effect of PF becomes more significant in stronger grids.

4. Conclusion

This paper aims to methodically analyse the stability boundary of GFL and GFM inverters based on a modified 3-bus testbench. The results of small-signal analysis are used to determine the system stability, thereby allowing the stability boundaries to be mapped in a "grid-search" manner. The proposed SBT algorithm facilitates identification and visualisation of the stability boundaries to assist theoretical understanding and system parameter selection.

The dynamic performance of GFL and GFM is comparatively assessed at different grid strengths, in conjunction to varying controller parameter. The main observations are summarized in Table III for ease of reference, indicating that some parameters yield similar impact and others opposite effect in GFL and GFM stability. In addition, further analysis on grid parameters shows that the resistive part of the transmission line has a positive effect on the system stability, but it is negligible for R/X ratios below 10%. Also, a lagging PF is beneficial for both GFL and GFM. Further work will extend this analysis to other inverter control variants and additional control functions, such as the Q-V control loop, and validate them in time-domain simulations.

5. Acknowledgements

This work has been conducted within UNIFORM project and supported by UKRI under Grant agreement EP/Y001575/1, and ROSES project (EP/T021713/1). It was also financially supported by the European Union's Horizon 2020 Research and Innovation Program and the Department of Science and Technology (DST), India through the RE-EMPOWERED Project under Grant Agreement No 101018420 and DST/TMD/INDIA/EU/ILES/2020/50(c) respectively.

6. References

[1] Han, F., Zhang, X., Li, M., et al.: 'Stability Control for Grid-Connected Inverters Based on Hybrid-Mode of Grid-Following and Grid-Forming', *IEEE Trans. Ind. Electron.*, 2023, pp. 1-11.

[2] IEEE Std 1204-1997: 'IEEE Guide for Planning DC Links Terminating at AC Locations Having Low Short-Circuit Capacities', 1997.

[3] Gao, X., Zhou, D., Blaabjerg, F., et al.: 'Stability analysis of grid-following and grid-forming converters based on state-space modelling', *IEEE Trans. Ind. Appl.*, 2024, pp. 1-12.

[4] Kong, L., Xue, Y., Qiao, L., et al.: 'Review of Small-Signal Converter-Driven Stability Issues in Power Systems', *IEEE Open Access J. Power Energy*, 2022, 9, pp. 29-41.

[5] Du, W., Chen, Z., Schneider, K. P., et al.: 'A comparative study of two widely used grid-forming droop controls on microgrid small-signal stability', *IEEE J. Emerg. Sel. Topics Power Electron.*, 2020, 8, (2), pp. 963-975.

[6] Zhou, J. Z., Ding, H., Fan, S., et al.: 'Impact of Short-Circuit Ratio and Phase-Locked-Loop Parameters on the Small-Signal Behavior of a VSC-HVDC Converter', *IEEE Trans. Power Deliv.*, 2014, 29, (5), pp. 2287-2296.

[7] Liu, F., Hu, L., Yuan, G., et al.: 'Control Loop Stability Criterion and Interaction Law Analysis for Grid-Connected Inverter in Weak Grid', *IEEE Access*, 2023, 11, pp. 12829-12842.

[8] Yu, J., Qi, Y., Deng, H., et al.: 'Evaluating small-signal synchronization stability of grid-forming converter: A geometrical approach', *IEEE Trans. Ind. Electron.*, 2022, 69, (9), pp. 9087-9098.

[9] Klein, M., Rogers, G.J., Kundur, P.: 'A Fundamental Study of Inter-Area Oscillations in Power Systems', *IEEE Trans. Power Syst.*, 1991, 6, (3), pp. 914–921.

[10] Canizares, C., Fernandes, T., Geraldi, E., et al.: 'Benchmark Models for the Analysis and Control of Small-Signal Oscillatory Dynamics in Power Systems', *IEEE Trans. Power Syst.*, 2016, 32, (1), pp. 715–722.

[11] Denis, G., Prevost, T., Debry, M.S., et al.: 'The Migrate project: the challenges of operating a transmission grid with only inverter-based generation. A grid-forming control improvement with transient current-limiting control', *IET Renew. Power Gener.*, 2018, 12, (5), pp. 523-529.

[12] Pogaku, N., Prodanovic, M., Green, T.C.: 'Modeling, Analysis and Testing of Autonomous Operation of an Inverter-Based Microgrid', *IEEE Trans. Power Electron.*, 2007, 22, (2), pp. 613–625.

[13] Singh, A.K., and Pal, B. C.: 'Dynamic estimation and control of power systems' (Academic Press, 2018).

[14] Huang, L., Wu, C., Zhou, D., et al.: 'A Double-PLLs-Based Impedance Reshaping Method for Extending Stability Range of Grid-Following Inverter Under Weak Grid', *IEEE Trans. Power Electron.*, 2022, 37, (4), pp. 4091-4104.

[15] Li, Y., Gu, Y., Green, T. C.: 'Revisiting grid-forming and grid-following inverters: A duality theory', IEEE Trans. Power Syst., 2022, 37, (6), pp. 4541-4554.

[16] Groß, D., Ramasubramanian, D., Paz, B.: 'Universal input-output model of GFM functions and data-driven verification methods', UNIFI-2022-4-1, 2022.